research paper

STRUCTURAL CHEMISTRY

ISSN 2053-2296

ss-NMR and single-crystal X-ray diffraction in the elucidation of a new polymorph of bischalcone (1*E*,4*E*)-1,5-bis(4-fluorophenyl)penta-1,4-dien-3-one

Lívia O. A. Ferreira, Ana Karoline S. M. Valdo, José Antônio Nascimento Neto, Leandro Ribeiro, Jefferson R. D. da Silva, Luiz H. K. Queiroz Jr., Caridad N. Perez and Felipe T. Martins*

Institute of Chemistry, Federal University of Goiás, Goiânia, GO 74001-970, Brazil. *Correspondence e-mail: felipetmartins@yahoo.com.br

Received 30 January 2019
Accepted 2 May 2019

Edited by A. G. Oliver, University of Notre Dame, USA

Keywords: polymorphism; crystal structure; packing; ss-NMR; bischalcone.

CCDC reference: 1913498

Supporting information: this article has supporting information at journals.iucr.org/c

We report a new polymorph of (1*E*,4*E*)-1,5-bis(4-fluorophenyl)penta-1,4-dien-3-one, $C_{17}H_{12}F_2O$. Contrary to the precedent literature polymorph with $Z' = 3$, our polymorph has one half molecule in the asymmetric unit disordered over two 50% occupancy sites. Each site corresponds to one conformation around the single bond vicinal to the carbonyl group (so-called *anti* or *syn*). The other half of the bischalcone is generated by twofold rotation symmetry, giving rise to two half-occupied and overlapping molecules presenting both *anti* and *syn* conformations in their open chain. Such a disorder allows for distinct patterns of intermolecular C—H···O contacts involving the carbonyl and *anti*-oriented *β*-C—H groups, which is reflected in three ^{13}C NMR chemical shifts for the carbonyl C atom. Here, we have also assessed the cytotoxicity of three symmetric bischalcones through their *in vitro* antitumour potential against three cancer cell lines. Cytotoxicity assays revealed that this biological property increases as halogen electronegativity increases.

1. Introduction

In recent years, the pharmaceutical industry has evaluated *ca* one million new molecules per year. However, releasing a new drug onto the market is challenging and demands many expensive and time-consuming steps. Only 20% of all new compounds are candidates for clinical trials and just 10% of those are registered (Liargkova *et al.*, 2016). Because of this, the search for potential drug candidates is a trend nowadays, enabling the design of useful molecular libraries in order to reduce high research costs. With this concern in mind, chalcones (1,3-diphenylprop-2-en-1-ones) have attracted attention as platforms for drug candidates. Chalcones are composed of a core benzophenone bonded to an enone group. Their biological activity is well established (Doriguetto *et al.*, 2007; Murata *et al.*, 2010). Therefore, chalcones represent an attractive class of compounds due to the combination of several structural, synthetic and pharmacological properties. The large number of replaceable H atoms can give rise to a wide range of derivatives while simultaneously promising biological activity through easy and high yield synthesis (Dimmock *et al.*, 1999). These remarkable structures have been widely studied as antiviral (Trivedi *et al.*, 2007), antifungal (Mobinikhaledi *et al.*, 2012), antioxidant (Iqbal *et al.*, 2014), anti-ulcerogenic (Yamamoto *et al.*, 1992) and anticancer (Solomon & Lee, 2012) agents. The symmetric bischalcones, a

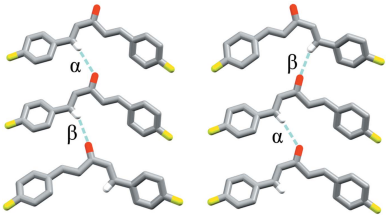

subclass of the chalcone family, are also known to present interesting biological activities, such as antimicrobial (Asiri & Khan, 2011), anticancer (Modzelewska *et al.*, 2006), radioprotective and antiviral (Singh & Raghav, 2014), as well as reducing glucose levels in the blood (Cai *et al.*, 2017). These properties make them attractive for the pharmaceutical industry.

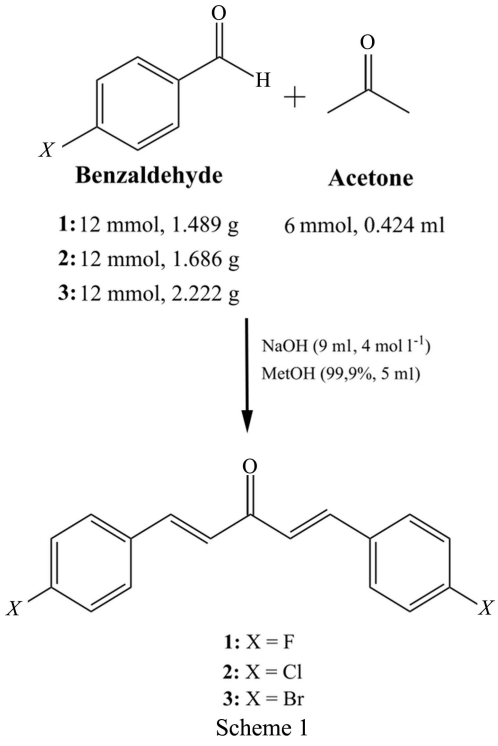

Scheme 1

Based on this, we have synthesized, characterized and evaluated the cytotoxicities of three symmetric bischalcones, namely, (1*E*,4*E*)-1,5-bis(4-fluorophenyl)penta-1,4-dien-3-one (**1**), (1*E*,4*E*)-1,5-bis(4-chlorophenyl)penta-1,4-dien-3-one (**2**) and (1*E*,4*E*)-1,5-bis(4-bromophenyl)penta-1,4-dien-3-one (**3**). Their cytotoxicities were assessed by their *in vitro* antitumour potential against three cancer cell lines, namely SNB-19 (glioblastoma), PC-3 (prostate) and HCT-116 (colon). All three compounds were previously reported in the literature (Butcher *et al.*, 2007, 2006; Aher *et al.*, 2011). In addition, during these studies, we have obtained single crystals of **1** and **2**. The unit cell for compound **1** did not match those of the known compounds. However, structural elucidation revealed this to be an interesting polymorphic modification of a previously described structure (Butcher *et al.*, 2007). Meanwhile, the single crystal of **2** showed the same unit-cell parameters as the reported structure for this compound (Butcher *et al.*, 2006). However, the polymorph reported herein has a cell volume one-third that of Butcher's reported structure and will be discussed in detail. It has one half molecule in the asymmetric unit, which is completely disordered over two sites of 50% occupancy (except for the carbonyl C atom) due to the conformational freedom around the single bond vicinal to the carbonyl group (the so-called *anti* or *syn* conformations). This disorder pattern and the occurrence of a twofold symmetry axis crossing through the carbonyl C atom generates an *anti*–*syn* (AS) conformer in the lattice, which can be assembled in a distinct manner into a C—H···O hydrogen-bonded chain. Furthermore, solid-state nuclear magnetic resonance (ss-NMR) has been important for describing the intermolecular interactions found in the new polymorph.

Table 1
Experimental details.

Crystal data	
Chemical formula	$C_{17}H_{12}F_2O$
M_r	270.27
Crystal system, space group	Monoclinic, *C*2/*c*
Temperature (K)	296
a, *b*, *c* (Å)	30.184 (3), 5.8907 (5), 7.7144 (6)
β (°)	98.040 (5)
V (Å^3)	1358.18 (19)
Z	4
Radiation type	Cu $K\alpha$
μ (mm^{-1})	0.84
Crystal size (mm)	0.15 × 0.10 × 0.10
Data collection	
Diffractometer	Bruker APEXII CCD
Absorption correction	Multi-scan (*SADABS*; Blessing, 1995)
T_{min}, T_{max}	0.744, 0.920
No. of measured, independent and observed [$I > 2\sigma(I)$] reflections	4490, 1148, 873
R_{int}	0.040
(sin $\theta/\lambda)_{max}$ (Å^{-1})	0.596
Refinement	
$R[F^2 > 2\sigma(F^2)]$, $wR(F^2)$, S	0.045, 0.129, 1.06
No. of reflections	1148
No. of parameters	177
H-atom treatment	H-atom parameters constrained
$\Delta\rho_{max}$, $\Delta\rho_{min}$ (e Å^{-3})	0.14, −0.13

Computer programs: *APEX2* (Bruker, 2003), *SAINT* (Bruker, 2003), *SHELXS2014* (Sheldrick, 2015*a*), *SHELXL2018* (Sheldrick, 2015*b*), *WinGX* (Farrugia, 1999), *publCIF* (Westrip, 2010) and *Mercury* (Macrae *et al.*, 2008).

2. Experimental

2.1. Synthesis

The title compounds were synthesized by an aldol condensation reaction (Scheme 1), where the respective benzaldehydes were diluted in methanol and then a sodium hydroxide solution was added slowly. The reaction was stirred at room temperature (25 °C) and the reaction progress was followed by thin-layer chromatography. After 1 h, the precipitate was filtered off and washed with water and methanol. The resulting product of each reaction was dissolved in ethanol and after slow evaporation of the solvent (one week, 25 °C), single crystals were formed. The yields were 48, 46 and 30% and the melting-point ranges were 424–425, 448–449 and 484–485 K for **1**, **2** and **3**, respectively. It is important to reinforce that all three compounds were described previously in the literature. In all previous references (Butcher *et al.*, 2006, 2007; Aher *et al.*, 2011), the syntheses were also performed by aldol condensation, with slight differences from the procedures reported here. These changes for compounds **1** and **2** (Butcher *et al.*, 2006, 2007) consisted of an excess of acetone and 2 h of reaction. The previously reported crystal-

lization of compound **1** (Butcher *et al.*, 2007) was also conducted by slow evaporation, however, with a solvent mixture of acetone and toluene (1:1 *v*/*v*). For compound **3** (Aher *et al.*, 2011), a cold bath was used to maintain a temperature in the range 20–25°C.

2.2. Single-crystal X-ray diffraction

Crystal data and refinement statistics of **1** are shown in Table 1. H atoms were placed in idealized positions after their identification in difference Fourier maps and were refined with fixed individual isotropic displacement parameters [U_{iso}(H) = 1.2U_{eq}(C)] using a riding model with C—H bond lengths of 0.93 Å. The whole bischalchone molecule was found to be disordered over two sites. Their site-occupancy factors were set at 0.5, which resulted in only the AS conformer. The distribution of the most relevant torsion angles describing the conformational features of the compound was searched for among the bischalcone structures deposited in the Cambridge Structural Database (CSD; Groom *et al.*, 2016) using the *ConQuest* tool and afterwards analyzed with *Mercury* (Macrae *et al.*, 2008).

2.3. ss-NMR

The solid-state ^{13}C NMR spectrum was measured on a Bruker Avance III 500 spectrometer, operating at 500.13 MHz for ^{1}H and 125.77 MHz for ^{13}C, equipped with a CP/MAS (Cross-Polarization/Magic Angle Spinning) 4 mm probe. The sample was packed in a 4 mm MAS zirconia rotor and the ^{13}C NMR experiment was acquired using a CP pulse sequence at 298 K. The deconvolution of the signals was performed in the *Topspin* (Version 3.5) software with a pseudo-Voigt profile.

2.4. Powder X-ray diffraction

Intensity data were acquired at 298 K using graphite-monochromated Cu $K\alpha$ radiation (λ = 1.5418 Å) generated at 40 kV and 30 mA on a Shimadzu XRD-6000 diffractometer (continuous θ–2θ scan mode with a scan speed of 2.000° min^{-1}, a collection step of 0.020°, a divergence slit at 1.000°, scattering slits at either 0.500 (1.00 to 5.00° in 2θ) or 1.000° (5.02 to 40.00° in 2θ), and a receiving slit at 0.300 mm.

2.5. Additional characterization

The ^{1}H and ^{13}C NMR experiments for compounds **1**–**3** in solution were measured at 298 K on a Bruker Avance III 500 spectrometer (Figs. S1 and S2 in the supporting information). The analytical conditions were 500.13 MHz for ^{1}H and 125.03 MHz for ^{13}C (5 mm *z*-gradient TBI probe), using chloroform-*d* (500 µl) to prepare a solution with 10 mg of each compound. The positive-ion high-resolution mass spectra were obtained on an Orbitrap Q-Exactive Focus mass spectrometer (Thermo Scientific, Bremen, Germany) equipped with a heated electrospray ion source (Fig. S3 in the supporting information). The parameters used were: spray voltage 3.5 kV; capillary temperature 350 °C; Fourier transform MS resolution 70 000; S-Lens Level 50.0; sheath gas 30 (arbitrary units). Mass spectra were acquired in continuous monitoring mode with a mass range of 100–1000. The solid products of compounds **1**–**3** were dissolved in methanol with the addition of formic acid (0.1%). The resulting solution was analyzed by direct infusion through the syringe pump (Hamilton 1750RN) at a flow rate of 4 µl min^{-1}. The data were evaluated with *XCALIBUR* software (Version 2.2 SP1; Thermo Scientific, Bremen, Germany). Transmission IR spectra were acquired using a Spectrum 400 FT–IR/FT–FIR spectrometer (PerkinElmer), in which the samples were analyzed as KBr pellets (Fig. S4 in the supporting information).

2.6. Theoretical calculations

The energies of the found conformer of **1** [*anti–syn* (AS)] and the other putative ones [*anti–anti* (AA) and *syn–syn* (SS)] were calculated using *GAUSSIAN* (Frisch *et al.*, 2009) at the B3LYP/6-31++G(d,p) level of theory (Stephens *et al.*, 1994). The input for each one of the three conformers was built-up in *Mercury* (Macrae *et al.*, 2008), and full optimization was carried out.

2.7. Evaluation of cytotoxicity

Cytotoxicity analysis of the compounds was performed using the colorimetric MTT assay, which is based on the conversion of 3-(4,5-dimethylthiazol-2-yl)-2,5-diphenyl-2*H*-tetrazolium bromide (MTT) in formazan blue by mitochondrial enzymes present only in metabolically active cells. The tumour cells used, *i.e.* SNB-19 (human glioblastoma), PC-3 (prostate cancer) and HCT-116 (colon cancer), were donated by the National Cancer Institute (USA) and cultured in RPMI 1640 medium supplemented with 10% of fetal bovine serum and the antibiotics streptomycin and penicillin at 1%. The tested compounds were diluted with sterile and pure dimethyl sulfoxide (DMSO) at 5 mg ml^{-1}. For IC_{50} determination, the samples were tested at increasing concentrations (0.39 to 52.37 µmol l^{-1}) in serial dilutions. Cells were plated at 0.1 × 10^{6} cells ml^{-1} for the SNB-19 and PC-3, and at 0.7 × 10^{5} cells ml^{-1} for the HCT-116 line. The plates were incubated for 72 h at 37 °C under a 5% CO_2 atmosphere. At the end of this period, they were centrifuged and the supernatant was removed. The MTT solution (150 µl) was then added and the plates were incubated for 3 h. The absorbance was read after dissolution of the precipitate with 150 µl of pure DMSO in a plate spectrophotometer at 595 nm. Doxorubicin was used as the positive control at concentrations ranging from 0.06 to 8.62 µmol l^{-1}, while pure DMSO was used as the negative control.

3. Results and discussion

3.1. Structure elucidation

The crystal structure of compound **1** was solved in the space group *C*2/*c* with half a molecule in the asymmetric unit (Fig. 1). As expected, an *E* stereochemistry was found around C7═C8. However, two conformations around the single C8—C9 bond can be found in the asymmetric unit, which resulted in two sets

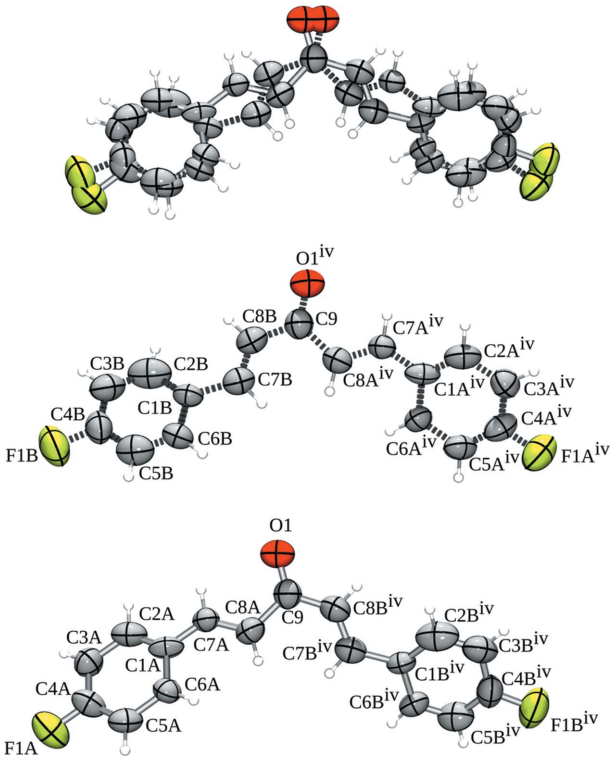

Figure 1
Compound **1** found in our polymorph, with both disordered sites represented by dashed and solid lines (top) and the separated sites (middle and bottom) featuring the AS conformer. [Symmetry code: (iv) $-x+1, y, -z+\frac{1}{2}$.]

of sites for the whole molecule (except for C9). Their occupancy, including C9, which is on a twofold symmetry axis, was constrained to 50%. Each set of sites corresponds to one conformation around the single bond vicinal to the carbonyl group (so-called *anti* or *syn*), which can be related by a rotation of *ca* 180° around the C8—C9 bond axis [O1—C9—C8*A*—C7*A* = 13.2 (7)° in the *anti* side and O1^{iv}—C9—C8*B*—C7*B* = −168.5 (6)° in the *syn* side; symmetry code: (iv) $-x+1, y, -z+\frac{1}{2}$]. The other half of the bischalcone is generated by twofold axis symmetry, giving rise to two half-occupied and overlapping molecules presenting both *anti* and *syn* conformations on the sides of their open chain (AS conformer). Such disorder present in the whole molecule is common for chalcones and occurs, for example, in (2*E*)-1-(2,4-dichlorophenyl)-3-[4-(prop-1-en-2-yl)phenyl]prop-2-en-1-one (Salian *et al.*, 2015). In addition, a similar case of polymorphism, also involving a bischalcone, namely 2,5-dibenzylidenecyclopent-3-en-1-one, was reported by Arshad *et al.* (2014). Both cases concern polymorphs with a variable value of Z', with no change in the conformation.

The carbon skeleton of compound **1** is not entirely planar in order to avoid repulsion between hydrogens (H2*A* and H7*A*, H2*B* and H8*B*, H6*A* and H8*A*, H6*B* and H7*B*, and H8*A* and H7*B*^{iv}). This can be expressed by the angle between the least-squares (l.s.) planes calculated through the planes defined by the propenone and arene moieties, which are 19.4 (17) and 20.8 (3)° for the *anti*- and *syn*-shaped sides, respectively. The planes were defined by C7*A*—C8*A*—C9—O1 [r.m.s. deviation (RMSD) = 0.186 Å], C7*B*—C8*B*—C9—O1^{iv} (RMSD = 0.176 Å), C1*A*—C2*A*—C3*A*—C4*A*—C5*A*—C6*A* (RMSD = 0.0307 Å) and C1*B*—C2*B*—C3*B*—C4*B*—C5*B*—C6*B* (RMSD = 0.0371 Å). In addition, the other two torsion angles on the C8—C9 single bond are 172.4 (4) (C7*A*—C8*A*—C9—C8*B*^{iv}) and 17.0 (6)° (C7*B*—C8*B*—C9—C8*A*^{iv}). Based on a search in the CSD (Version 5.39, May 2018; Groom *et al.*, 2016) for the torsion angle C7—C8—C9—C8^{iv} in similar bischalcones (Fig. 2), we see that most bischalcones present angles close to 0 or 180°, indicating a tendency towards coplanarity in the open chain. If we inspect *p*-fluorobischalcones (coloured red in the histograms of Fig. 2), the C7—C8—C9—C8 torsion angles are in the range 162–180° (18 of 24 molecules), corresponding to the AA and AS conformers present with the preferred *anti* conformation around C8—C9. On the other hand, the C6—C1—C7—C8 torsion can have a wider range of values, although coplanarity between the arene ring and the central propenone group is still preferred, since a larger number of related molecules is present with this torsion measuring 0 or 180°.

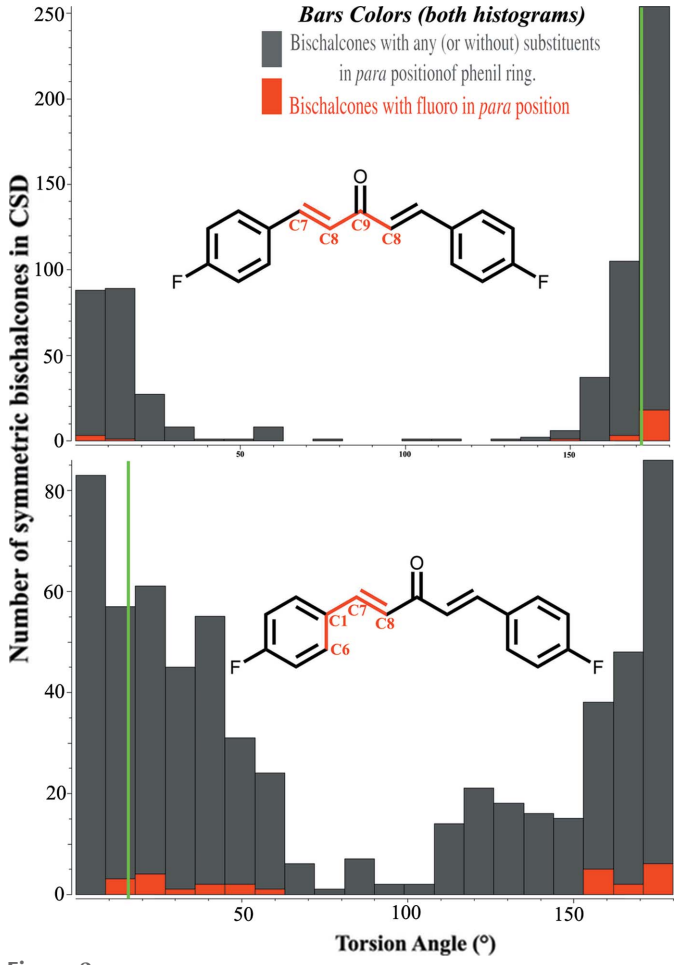

Figure 2
Distribution of the C7—C8—C9—C8 and C6—C1—C7—C8 torsion angles in the symmetric bischalcones present in the CSD. Green lines represent the values found in our polymorph of **1** for C7*A*—C8*A*—C9—C8*B*^{iv} [−172.4 (4)°; symmetry code: (iv) $-x+1, y, -z+\frac{1}{2}$] and C6*A*—C1*A*—C7*A*—C8*A* [16.8 (10)°].

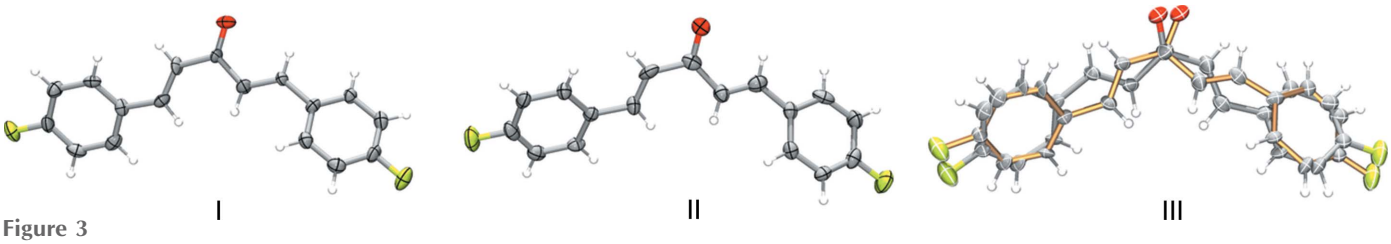

Figure 3
Crystallographically independent molecules found in the structure of the first polymorph of compound **1** (Butcher *et al.*, 2007).

Compound **1** is known to crystallize with three independent molecules (Z' = 3) in the *Cc* space group (Butcher *et al.*, 2007) (Fig. 3). This structure was elucidated in 2007 and no polymorph has been reported until now. Indeed, this phenomenon is not very common in chalcones and bischalcones because of an apparent rigidity in the conformation of the open-chain backbone (Ramos *et al.*, 2016; Jasinski *et al.*, 2009). In this precedent structure, only the AS conformer was found. One of the two crystallographically independent molecules also exhibits disorder, with occupancies of 0.6844 (16) and 0.3156 (16). The coplanarity is maintained, where the aforementioned angle between the propenone and arene moieties in the *anti*- and *syn*-shaped sides are respectively 28.17 (12) and 23.6 (2)° for molecule I, 26.2 (2) and 27.9 (9)° for II, 25.(5) and 24.5 (3)° for one disordered part of III, and 23.9 (17) and 25.8 (10)° for the second disorder component (Fig. 3). The RMSD values of the planes fitted through the propenone group and the arene ring range from 0.0562 to 0.131 Å, and from 0.00120 to 0.0194 Å in the *anti* and *syn* sides, respectively.

Table 2
Hydrogen-bond geometry (Å, °).

D—H···A	D—H	H···A	D···A	D—H···A
C3A—H3A···F1A^{i}	0.93	2.59	3.437 (17)	151
C3A—H3A···F1B^{i}	0.93	2.66	3.477 (17)	146
C3B—H3B···F1A^{i}	0.93	2.82	3.563 (19)	138
C3B—H3B···F1B^{i}	0.93	2.71	3.519 (19)	146
C7B—H7B···O1^{ii}	0.93	2.84	3.745 (6)	163
C7B—H7B···O1^{iii}	0.93	2.59	3.448 (4)	154

Symmetry codes: (i) $-x+\frac{3}{2}, y+\frac{1}{2}, -z+\frac{1}{2}$; (ii) $-x+1, y-1, -z+\frac{1}{2}$; (iii) $x, y-1, z$.

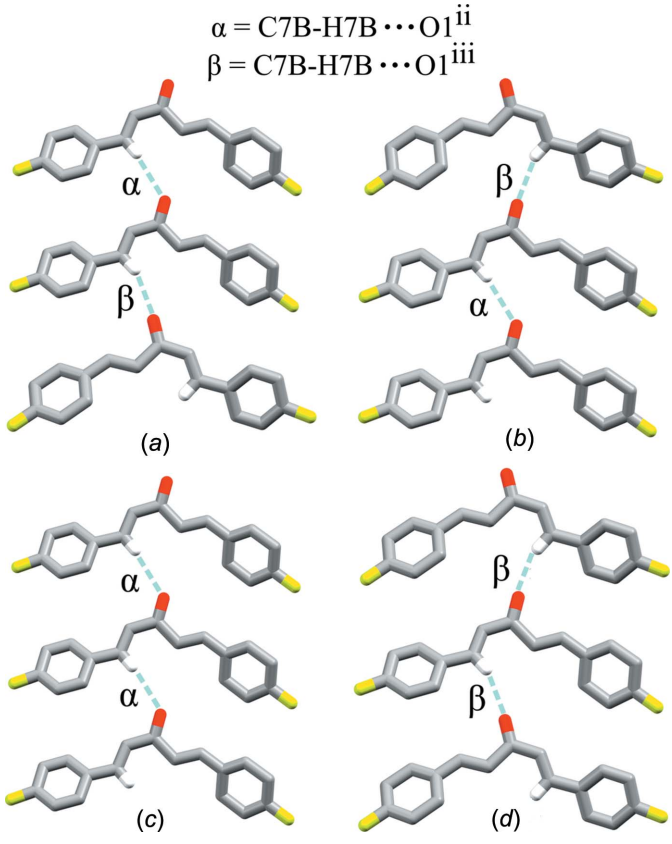

Figure 4
Representation of the C—H···O hydrogen-bonded triads forming $C(5)$ motifs in our polymorph of **1**. Each molecule can present four distinct environments (*a*)–(*d*), constructed from a combination of α and β labelled contacts for the middle molecule. Blue dashed lines indicate C—H···O interactions. [Symmetry codes: (ii) $-x+1, y-1, -z+\frac{1}{2}$; (iii) $x, y-1, z$.]

Regarding the crystal packing, the C—H···O contact is the main intermolecular interaction in **1**. This contact involves the β-C—H motif of the *anti* side and the carbonyl group as nonclassical hydrogen-bonding donor and acceptor, respectively, assembling the $C(5)$ synthon (Fig. 4). Due to the aforementioned disorder overlapping two half-occupied bischalcone molecules, which can be related by a twofold symmetry axis splitting them through atom C9, four distinct patterns of intermolecular C—H···O contacts can be experienced by a molecule in the lattice (Fig. 4). These are the combination of two geometrically different C7B—H7B···O1 contacts, which were labelled in Fig. 4 as α [C7B—H7B···O1^{ii}; symmetry code: (ii) $-x+1, y-1, -z+\frac{1}{2}$] and β [C7B—H7B···O1^{iii}; symmetry code: (iii) $x, y-1, z$]. ss-NMR has corroborated the occurrence of such patterns in the crystal structure of **1**. The ^{13}C ss-NMR spectrum of **1** is shown in Fig. 5 (the full spectrum is depicted in Fig. S5 in the supporting information), where three chemical shifts can be attributed to

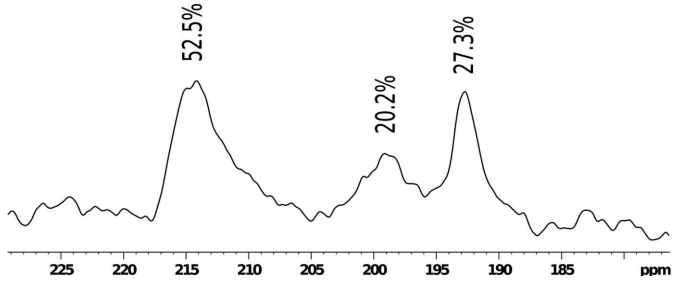

Figure 5
The ^{13}C ss-NMR spectrum in the carbonyl region.

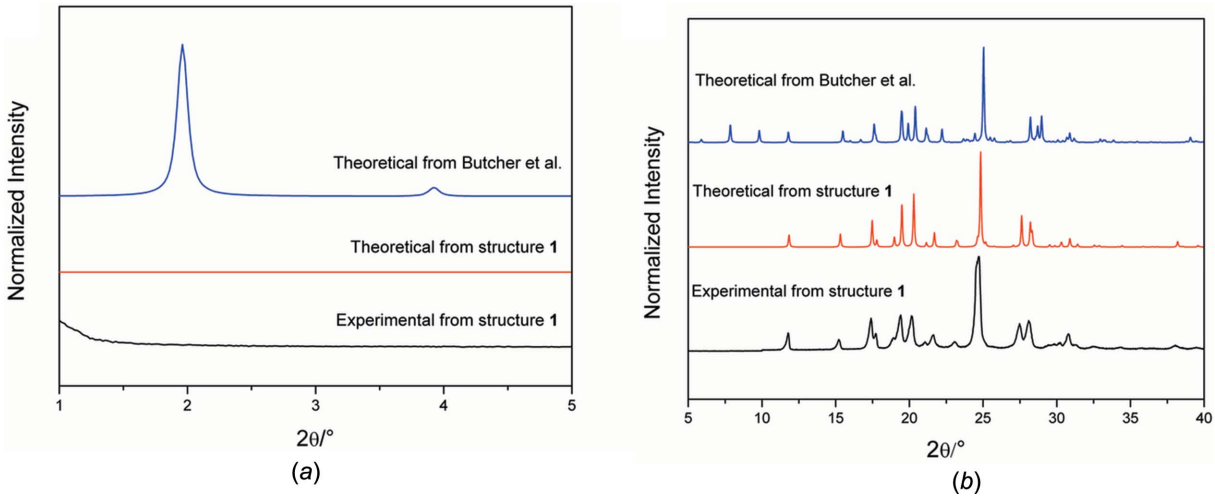

Figure 6
Experimental and simulated powder X-ray diffractograms of compound **1**. Due to the extremely high intensity of the peak at *ca* 2° in 2θ, the diffractrograms were split into two ranges of 2θ angles, *i.e.* (*a*) low (1.00 to 5.00°) and (*b*) high (5.02 to 40.00°).

C9 and therefore there are three chemical environments around it. These signals are centred at 192.5, 198.7 and 213.4 ppm. The peak integrals ascertained their relative occurrence as 27.3, 20.2 and 52.5%, respectively. In an attempt to assign these signals to the intermolecular contact patterns, we will infer the effect of such interactions in the C9 nucleus with respect to the degree of shielding by electrons. The signal at 192.5 ppm corresponds to the highest shielding, *i.e.* the C9 nucleus undergoes the lowest electron withdrawing around it. This is compatible with atom O1 withdrawing less electron density from C9 and an improved π-conjugation from C7*B* towards C9 as a function of the increase of the acidity of H7*B*. These two cases need O1 to accept a larger H···O distance in the C—H···O contact (α contact, H···O distance in Table 2) and C7*B*—H7*B* to participate with a shorter H···O distance (β contact, H···O distance in Table 2). Therefore, this NMR shift can be attributed to the middle molecule of Fig. 4(*a*). On the other hand, the signal at 213.4 ppm corresponds to the lowest C9 nucleus shielding, with O1 accepting a shorter H···O distance (β contact) and C7*B*—H7*B* engaged with a longer H···O distance (α contact). This molecule can be viewed in the middle panel of Fig. 4(*b*). In turn, if both atom O1 and the C7*B*—H7*B* group of the same molecule are involved in either larger (α contacts, Fig. 4*c*) or shorter (β contacts, Fig. 4*d*) H···O interactions, these electron-withdrawing and electron-donating effects towards C9 are compensated, and the C9 nucleus will experience a similar shielding that is intermediate between the two previous ones (corresponding to the broader signal at 198.7 ppm). It is important to mention that although the H7*B*···O1 distance in the α contact was larger than the sum of the van der Waals (vdW) radii, meaning a very weak contact, atom H7*B* is the β-hydrogen of a α,β-unsaturated ketone system, having an increased acidity which justifies its role in the *C*(5) motif assembly.

Since the literature polymorph could have been formed concomitantly to that reported here, leading to detection of three ^{13}C ss-NNM signals for C9 due to Z' = 3 (meaning three

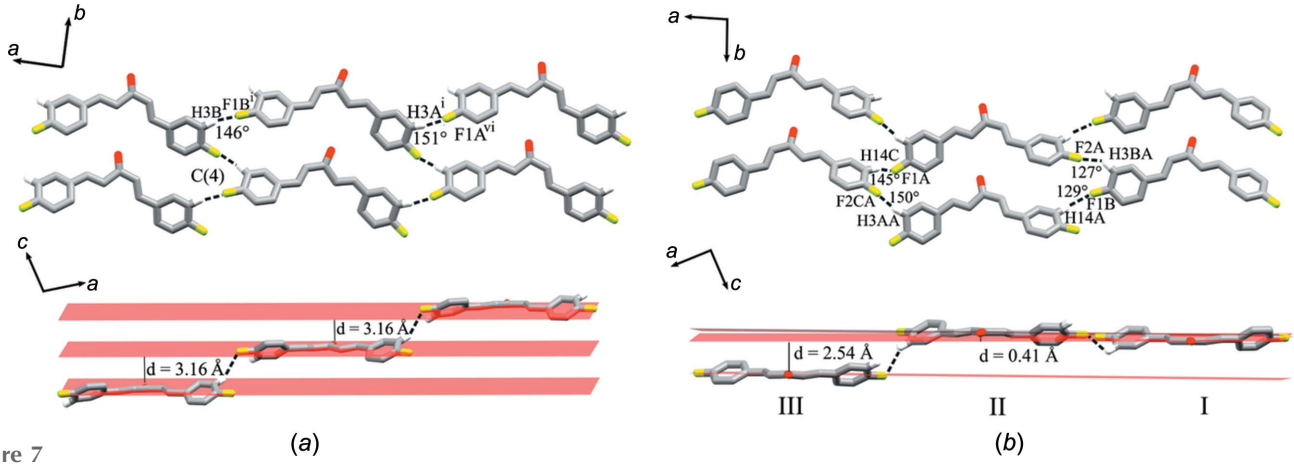

Figure 7
C—H···F interactions on the *ab* plane, showing the hydrogen-bonding angle and the displacement between the chains along the *c* axis for (*a*) the polymorph described here and (*b*) that from the literature (Butcher *et al.*, 2007). The shown molecular displacements were calculated between the least-squares plane fitted through all the non-H bischalcone atoms and the O atom of a neighbouring molecule. [Symmetry codes: (i) $-x+\frac{3}{2}, y+\frac{1}{2}, -z+\frac{1}{2}$; (vi) $-x+2, y+1, -z+\frac{1}{2}$.]

Table 3
Determination of the IC_{50} (μmol l^{-1}) of synthetic bischalcones against tumour cell lines.

The trust range was 95% and NT denotes not tested.

Compound	PC3	HCT-116	SnB19
1	18.74 (17.11–20.59)	5.15 (4.48–5.89)	27.00 (24.44–29.85)
2	32.55 (28.28–37.48)	8.01 (7.19–8.97)	43.18 (38.08–49.01)
3	>60	12.98 (11.48–14.71)	>60
Doxorubicin	0.81 (0.63–0.99)	0.22 (0.17–0.31)	NT

chemical environments), we have performed a powder X-ray diffraction analysis on the same sample from which our analyzed single crystal was isolated and on which the ss-NMR spectrum was acquired. The experimental powder X-ray diffractogram was performed for the new polymorph and then compared with the theoretical diffractograms simulated with *Mercury* (Macrae *et al.*, 2008) for both polymorphs. As can be seen in the low 2θ region of the diffractogram (Fig. 6*a*), there are peaks only for the literature polymorph (Butcher *et al.*, 2007). This is caused due to the presence of a large interplanar spacing, evidenced by the long unit-cell length *a* of 90.019 (14) Å. Those initial peaks (*ca* 2 and 4° in 2θ) correspond to the (200) and (400) planes. This difference is still observed in the range of 2θ from 5 to 10° (Fig. 6*b*). Meanwhile, with an increase of the 2θ value, the diffraction patterns of the two polymorphs become similar. Even so, some peaks are still present only in the polymorph reported by Butcher *et al.* (2007), such as those around 20 and 28° in 2θ. Therefore, the experimental diffractogram was overlaid with the simulated profile from our crystal structure and that simulated from the literature structure (Fig. 6), allowing one to conclude that these two structures are doubtless distinct polymorphs and that the literature polymorph is not present concomitantly with the polymorph we report here.

The explanation of the three NMR signals based on the C—H···O interactions is further justified taking into account the energetic relevance of such contacts for this compound. Preferably, in the gas phase, the molecules mostly have an *anti* conformation in both molecular sides (AA conformer) because of its lower energy. The fully optimized AS and SS (the last with a *syn* conformation in both molecular sides) conformers of **1** at the B3LYP/6-31++G(d,p) level of theory present an energy higher than that of the lowest energy AA conformer by 2.0 and 4.6 kcal mol^{-1}, respectively. Therefore, the presence of the C—H···O hydrogen bonding justifies the presence of the higher energy AS conformer in the solid state and changes in the geometry of these contacts can change the shielding of the C9 nucleus, since these are responsible for stablizing a higher energy conformer in the solid state.

Besides the C—H···O interaction, another nonclassical hydrogen bond is found between bischalcone molecules. This contact is of the type C—H···F and is responsible for the formation of *C*(4) motifs on both sides of all molecules (Fig. 7). In comparison to the previously reported structure of **1** (Butcher *et al.*, 2007), the aforementioned *C*(5) and *C*(4) motifs are conserved. Nevertheless, there are other subtle differences in the packing of both structures, as will be discussed in sequence.

As can be seen in Fig. 7, in the packing of both polymorphs of **1**, chains running along the [100] and [010] directions formed through C—H···F contacts are present. Fig. 7(*a*) was built-up only with C3*A*—H3*A*···F1*A* and C3*B*—H3*B*···F1*B* contacts. The geometries of the C—H···F contacts are summarized in Table 2 (our polymorph) and in Table S1 of the supporting information (literature polymorph). All the metrics for these nonclassical hydrogen bonds reveal a better directionality of the contacts in our polymorph than in that of Butcher's polymorph (*e.g.* the C—H···F angles are closer to 180° herein; Fig. 7 and Table 2, and Table S1 of the supporting information). The metrics for these intermolecular interactions are within the expected range (Shukla & Chopra, 2015). This improvement in the angles of the C—H···F contacts may indicate more stability of our polymorph compared with the literature form, which agrees well with the lower Z' value in the crystal form reported here due to optimization of the geometry of the intermolecular contacts for all molecules (Desiraju, 2007). The polymorphism phenomenon is also seen in an intermolecular fashion when comparing the structures on the (010) plane. The arrangement of the C—H···F hydrogen-bonded chains can be described as ladder-like in our polymorph, wherein the molecules are disposed side-by-side, with a regular displacement of 3.16 Å (Fig. 7*a*). This displacement was calculated as being the distance between the l.s. plane fitted through all non-H bischalcone atoms and the O atom of a neighbouring molecule (because molecular planes are not perfectly planar in the previous polymorph). In the structure described here, this displacement is the same along the *c* axis. Meanwhile, in the previously reported structure (Butcher *et al.*, 2007), there are different values for such this displacement (*i.e.* the distance between the mentioned l.s. planes), even being negligible for the corresponding distance between molecules I and II. These distances were calculated for the previously reported structure (Butcher *et al.*, 2007), resulting in values of 2.54 (between the l.s. plane of I and the major-occupancy O atom of III), 3.53 (between the l.s. plane of II and the major-occupancy O atom of III) and 0.41 Å (between the l.s. plane of I and the O atom of II), as illustrated in Fig. 7(*b*).

3.2. Cytotoxicity assay

All three compounds were tested for cytotoxic potential against three tumour cell lines. Initially, the compounds were tested at a single concentration of 25 μg ml^{-1} against the tumour cell lines.

All compounds had a percentage of tumour growth inhibition greater than 75% against all tumour cell lines tested, except for compound **3** which had an inhibition less than 75% against PC-3 and SNB-19 cells. The compounds were then diluted for the IC_{50} determination. To evaluate the cytotoxic

potential, these compounds were tested together with a reference standard, *i.e.* doxorubicin, a drug widely used in cancer chemotherapy (Table 3). Negative control (pure DMSO) has not inhibited cell growth.

Compounds **1** and **2** showed good cytotoxic effect against all tumour cell lines tested, with IC_{50} values ranging from 18.74 to 32.55 µmol l^{-1} against the PC-3 lineage, from 5.15 to 8.01 µmol l^{-1} against HCT-116 and from 27.00 to 43.18 µmol l^{-1} against SNB-19. Compound **3** showed significant cytotoxicity only against the HCT-116 line, with an IC_{50} value of 12.98 µmol l^{-}. By inspection of Table 3, it is possible to see that the IC_{50} values increase from the fluoro to the bromo substituent against all three cell lines. Therefore, a tentative structure–activity relationship states that the cytotoxicity of the *p*-halogen symmetric bischalcones increases with increasing halogen electronegativity. Other bischalcones related to **1**–**3** have already presented an inhibitory effect on the PC-3 prostate, Panc-1 pancreas and HT-29 colon cancer cell lines, including similar IC_{50} values ranging from 13.12 to 37.23 µmol l^{-1} for PC-3 and from 6.24 to 36.08 µmol l^{-1} for HT-29 (Khazaei *et al.*, 2016). Furthermore, as observed here, in this previous work (Khazaei *et al.*, 2016), it was also found that the cytotoxicity of the *p*-halogenated symmetric bischalcones increases according to halogen electronegativity.

Acknowledgements

The authors acknowledge CNPq, CAPES, FAPEMIG and FAPEG for financial support and research fellowships.

References

Aher, R. B., Wanare, G., Kawathekar, N., Kumar, R. R., Kaushik, N. K., Sahal, D. & Chauhan, V. S. (2011). *Bioorg. Med. Chem. Lett.* **21**, 3034–3036.
Arshad, I., Ashraf, S., Abbas, A., Hameed, S., Lo, K. M. & Naseer, M. M. (2014). *Eur. Chem. Bull.* **3**, 587–592.
Asiri, A. M. & Khan, S. A. (2011). *Molecules*, **16**, 523–531.
Blessing, R. H. (1995). *Acta Cryst.* A**51**, 33–38.
Bruker (2003). *APEX2* and *SAINT*. Bruker AXS Inc., Madison, Wisconsin, USA.
Butcher, R. J., Jasinski, J. P., Sarojini, B. K., Yathirajan, H. S., Bindya, S. & Narayana, B. (2007). *Acta Cryst.* E**63**, o3213–o3214.
Butcher, R. J., Yathirajan, H. S., Sarojini, B. K., Narayana, B. & Vijaya Raj, K. K. (2006). *Acta Cryst.* E**62**, o1973–o1975.
Cai, C. Y., Rao, L., Rao, Y., Guo, J. X., Xiao, Z. Z., Cao, J. Y., Huang, Z. S. & Wang, B. (2017). *Eur. J. Med. Chem.* **130**, 51–59.
Desiraju, G. R. (2007). *Angew. Chem. Int. Ed.* **46**, 8342–8356.
Dimmock, J. R., Elias, D. W., Beazely, M. A. & Kandepu, N. M. (1999). *Curr. Med. Chem.* **6**, 1125–1149.
Doriguetto, A. C., Martins, F. T., Ellena, J., Salloum, R., dos Santos, M. H., Moreira, M. E., Schneedorf, J. M. & Nagem, T. J. (2007). *Chem. Biodivers.* **4**, 488–499.
Farrugia, L. J. (1999). *J. Appl. Cryst.* **32**, 837–838.
Frisch, M. J., *et al.* (2009). *GAUSSIAN*. Gaussian Inc., Wallingford, CT, USA. http://www.gaussian.com.
Groom, C. R., Bruno, I. J., Lightfoot, M. P. & Ward, S. C. (2016). *Acta Cryst.* B**72**, 171–179.
Iqbal, H., Prabhakar, V., Sangith, A., Chandrika, B. & Balasubramanian, R. (2014). *Med. Chem. Res.* **23**, 4383–4394.
Jasinski, J. P., Butcher, R. J., Veena, K., Narayana, B. & Yathirajan, H. S. (2009). *Acta Cryst.* E**65**, o1965–o1966.
Khazaei, A., Sarmasti, N. & Seyf, J. Y. (2016). *J. Mol. Struct.* **1108**, 168–178.
Liargkova, T., Hadjipavlou-Litina, D. J., Koukoulitsa, C., Voulgari, E. & Avgoustakis, C. (2016). *J. Enzyme Inhib. Med. Chem.* **31**, 302–313.
Macrae, C. F., Bruno, I. J., Chisholm, J. A., Edgington, P. R., McCabe, P., Pidcock, E., Rodriguez-Monge, L., Taylor, R., van de Streek, J. & Wood, P. A. (2008). *J. Appl. Cryst.* **41**, 466–470.
Mobinikhaledi, A., Kalhor, M. & Jamalifar, H. (2012). *Med. Chem. Res.* **21**, 1811–1816.
Modzelewska, A., Pettit, C., Achanta, G., Davidson, N. E., Huang, P. & Khan, S. R. (2006). *Bioorg. Med. Chem.* **14**, 3491–3495.
Murata, R. M., Yatsuda, R., dos Santos, M. H., Kohn, L. K., Martins, F. T., Nagem, T. J., Alencar, S. M., de Carvalho, J. E. & Rosalen, P. L. (2010). *Phytother. Res.* **24**, 379–383.
Ramos, R. R., da Silva, C. C., Guimarães, F. F. & Martins, F. T. (2016). *CrystEngComm*, **18**, 2144–2154.
Salian, V. V., Narayana, B., Yathirajan, H. S., Akkurt, M., Çelik, Ö., Ersanli, C. C. & Glidewell, C. (2015). *Acta Cryst.* C**71**, 610–617.
Sheldrick, G. M. (2015*a*). *Acta Cryst.* A**71**, 3–8.
Sheldrick, G. M. (2015*b*). *Acta Cryst.* C**71**, 3–8.
Shukla, R. & Chopra, D. (2015). *CrystEngComm*, **17**, 3596–3609.
Singh, M. & Raghav, N. (2014). *Med. Chem. Res.* **23**, 1781–1788.
Solomon, V. R. & Lee, H. (2012). *Biomed. Pharmacother.* **66**, 213–220.
Stephens, P. J., Devlin, F. J., Chabalowski, C. F. & Frisch, M. J. (1994). *J. Phys. Chem.* **98**, 11623–11627.
Trivedi, J. C., Bariwal, J. B., Upadhyay, K. D., Naliapara, Y. T., Joshi, S. K., Pannecouque, C. C., De Clercq, E. & Shah, A. K. (2007). *Tetrahedron Lett.* **48**, 8472–8474.
Westrip, S. P. (2010). *J. Appl. Cryst.* **43**, 920–925.
Yamamoto, K., Kakegawa, H., Ueda, H., Matsumoto, H., Sudo, T., Miki, T. & Satoh, T. (1992). *Planta Med.* **58**, 389–393.

supporting information

Acta Cryst. (2019). C**75** [https://doi.org/10.1107/S2053229619006156]

ss-NMR and single-crystal X-ray diffraction in the elucidation of a new polymorph of bischalcone (1*E*,4*E*)-1,5-bis(4-fluorophenyl)penta-1,4-dien-3-one

Lívia O. A. Ferreira, Ana Karoline S. M. Valdo, José Antônio Nascimento Neto, Leandro Ribeiro, Jefferson R. D. da Silva, Luiz H. K. Queiroz, Caridad N. Perez and Felipe T. Martins

Computing details

Data collection: *APEX2* (Bruker, 2003); cell refinement: *SAINT* (Bruker, 2003); data reduction: *SAINT* (Bruker, 2003); program(s) used to solve structure: *SHELXS2014* (Sheldrick, 2015a); program(s) used to refine structure: *SHELXL2018* (Sheldrick, 2015b); molecular graphics: *WinGX* (Farrugia, 1999); software used to prepare material for publication: *publCIF* (Westrip, 2010) and *Mercury* (Macrae *et al.*, 2008).

(1*E*,4*E*)-1,5-Bis(4-fluorophenyl)penta-1,4-dien-3-one

Crystal data

$C_{17}H_{12}F_2O$
$M_r = 270.27$
Monoclinic, $C2/c$
$a = 30.184$ (3) Å
$b = 5.8907$ (5) Å
$c = 7.7144$ (6) Å
$\beta = 98.040$ (5)°
$V = 1358.18$ (19) Å^3
$Z = 4$
$F(000) = 560$
$D_x = 1.322$ Mg m^{-3}
Cu $K\alpha$ radiation, $\lambda = 1.54178$ Å
Cell parameters from 1008 reflections
$\theta = 8.7$–66.1°
$\mu = 0.84$ mm^{-1}
$T = 296$ K
Prism, yellow
0.15 × 0.10 × 0.10 mm

Data collection

Bruker APEXII CCD diffractometer
CCD scans
Absorption correction: multi-scan (SADABS; Blessing, 1995)
$T_{min} = 0.744$, $T_{max} = 0.920$
4490 measured reflections
1148 independent reflections
873 reflections with $I > 2\sigma(I)$
$R_{int} = 0.040$
$\theta_{max} = 66.8°$, $\theta_{min} = 8.7°$
$h = -34\rightarrow35$
$k = -7\rightarrow6$
$l = -8\rightarrow9$

Refinement

Refinement on F^2
Least-squares matrix: full
$R[F^2 > 2\sigma(F^2)] = 0.045$
$wR(F^2) = 0.129$
$S = 1.06$
1148 reflections
177 parameters
0 restraints
Primary atom site location: structure-invariant direct methods
Secondary atom site location: difference Fourier map
Hydrogen site location: inferred from neighbouring sites
H-atom parameters constrained

$w = 1/[\sigma^2(F_o^2) + (0.0631P)^2 + 0.1789P]$
where $P = (F_o^2 + 2F_c^2)/3$
$(\Delta/\sigma)_{max} < 0.001$

$\Delta\rho_{max} = 0.14$ e Å^{-3}
$\Delta\rho_{min} = -0.13$ e Å^{-3}

Special details

Geometry. All esds (except the esd in the dihedral angle between two l.s. planes) are estimated using the full covariance matrix. The cell esds are taken into account individually in the estimation of esds in distances, angles and torsion angles; correlations between esds in cell parameters are only used when they are defined by crystal symmetry. An approximate (isotropic) treatment of cell esds is used for estimating esds involving l.s. planes.

Fractional atomic coordinates and isotropic or equivalent isotropic displacement parameters (Å²)

	x	*y*	*z*	U_{iso}*/U_{eq}	Occ. (<1)
C4A	0.6814 (8)	0.099 (4)	0.085 (2)	0.080 (4)	0.5
C5A	0.6399 (8)	0.014 (3)	0.044 (2)	0.078 (4)	0.5
H5A	0.635009	−0.130419	−0.004262	0.094*	0.5
C2A	0.6525 (8)	0.444 (3)	0.191 (3)	0.082 (3)	0.5
H2A	0.657795	0.590749	0.232641	0.098*	0.5
C6A	0.6024 (5)	0.1616 (17)	0.0799 (17)	0.067 (2)	0.5
H6A	0.572993	0.113930	0.049982	0.080*	0.5
C8B	0.5441 (2)	0.5655 (9)	0.2198 (5)	0.0741 (11)	0.5
H8B	0.566127	0.676994	0.225990	0.089*	0.5
C9	0.500000	0.6399 (4)	0.250000	0.0739 (6)	
C1A	0.6118 (4)	0.3755 (14)	0.1597 (11)	0.068 (2)	0.5
C3A	0.6907 (6)	0.304 (3)	0.165 (2)	0.078 (3)	0.5
H3A	0.719934	0.351665	0.201368	0.094*	0.5
C7A	0.57605 (12)	0.5132 (6)	0.1977 (3)	0.0606 (7)	0.5
H7A	0.583197	0.665009	0.219610	0.073*	0.5
C7B	0.55635 (17)	0.3624 (6)	0.1855 (4)	0.0718 (8)	0.5
H7B	0.535252	0.247067	0.184062	0.086*	0.5
C8A	0.53286 (18)	0.4571 (11)	0.2071 (5)	0.0719 (10)	0.5
H8A	0.523243	0.308082	0.187627	0.086*	0.5
F1B	0.7249 (2)	0.0741 (8)	0.0571 (10)	0.1296 (17)	0.5
C2B	0.6426 (8)	0.427 (3)	0.207 (3)	0.101 (7)	0.5
H2B	0.640642	0.557907	0.272500	0.121*	0.5
F1A	0.7162 (2)	−0.0331 (7)	0.0539 (9)	0.1216 (16)	0.5
C3B	0.6810 (6)	0.362 (3)	0.170 (3)	0.091 (4)	0.5
H3B	0.706072	0.453802	0.196703	0.109*	0.5
C5B	0.6471 (8)	0.031 (3)	0.034 (2)	0.088 (6)	0.5
H5B	0.649620	−0.101089	−0.029744	0.105*	0.5
C1B	0.6027 (3)	0.2985 (14)	0.1472 (11)	0.0596 (16)	0.5
C6B	0.6088 (5)	0.093 (2)	0.0673 (17)	0.066 (2)	0.5
H6B	0.584355	−0.001676	0.037142	0.079*	0.5
C4B	0.6846 (7)	0.157 (4)	0.090 (2)	0.084 (5)	0.5
O1	0.5095 (2)	0.8393 (4)	0.2453 (17)	0.1042 (17)	0.5

Atomic displacement parameters (Å²)

	U^{11}	U^{22}	U^{33}	U^{12}	U^{13}	U^{23}
C4A	0.099 (8)	0.072 (7)	0.067 (4)	0.021 (5)	0.004 (4)	−0.009 (4)
C5A	0.096 (8)	0.054 (4)	0.081 (7)	0.001 (5)	−0.001 (5)	0.005 (4)
C2A	0.116 (8)	0.054 (4)	0.075 (7)	0.001 (5)	0.007 (5)	0.002 (4)
C6A	0.070 (4)	0.055 (7)	0.074 (4)	0.010 (4)	0.008 (3)	0.005 (4)
C8B	0.085 (4)	0.065 (3)	0.072 (2)	−0.010 (2)	0.0129 (18)	0.0033 (19)
C9	0.0732 (15)	0.0795 (14)	0.0696 (12)	0.000	0.0120 (9)	0.000
C1A	0.104 (6)	0.044 (4)	0.050 (2)	−0.008 (3)	−0.005 (2)	−0.004 (3)
C3A	0.072 (4)	0.080 (10)	0.080 (3)	−0.006 (5)	0.006 (3)	−0.002 (5)
C7A	0.070 (2)	0.0509 (17)	0.0624 (14)	−0.0034 (18)	0.0138 (13)	−0.0015 (11)
C7B	0.085 (3)	0.064 (2)	0.0647 (17)	−0.006 (2)	0.0035 (16)	0.0017 (14)
C8A	0.079 (3)	0.063 (3)	0.073 (2)	−0.011 (3)	0.0124 (17)	−0.0020 (19)
F1B	0.094 (3)	0.149 (4)	0.154 (3)	0.036 (3)	0.046 (2)	0.017 (4)
C2B	0.165 (17)	0.079 (8)	0.059 (4)	0.001 (8)	0.015 (7)	−0.008 (5)
F1A	0.114 (3)	0.122 (3)	0.127 (2)	0.038 (3)	0.0131 (19)	−0.015 (3)
C3B	0.105 (12)	0.064 (8)	0.099 (5)	−0.006 (6)	0.001 (6)	0.006 (5)
C5B	0.126 (13)	0.078 (9)	0.060 (4)	0.000 (6)	0.019 (5)	−0.006 (4)
C1B	0.077 (4)	0.046 (5)	0.056 (2)	0.007 (3)	0.010 (3)	−0.004 (3)
C6B	0.078 (6)	0.056 (6)	0.065 (2)	0.013 (4)	0.008 (2)	0.001 (4)
C4B	0.066 (4)	0.098 (14)	0.092 (7)	0.010 (6)	0.023 (5)	0.019 (7)
O1	0.105 (6)	0.0680 (12)	0.142 (2)	0.0007 (13)	0.026 (5)	−0.0001 (18)

Geometric parameters (Å, º)

C4A—C5A	1.35 (4)	C3A—H3A	0.9300
C4A—F1A	1.36 (2)	C7A—C8A	1.357 (7)
C4A—C3A	1.37 (3)	C7A—H7A	0.9300
C5A—C6A	1.48 (2)	C7B—C1B	1.518 (10)
C5A—H5A	0.9300	C7B—H7B	0.9300
C2A—C1A	1.28 (3)	C8A—H8A	0.9300
C2A—C3A	1.45 (2)	F1B—C4B	1.37 (2)
C2A—H2A	0.9300	C2B—C3B	1.29 (2)
C6A—C1A	1.414 (11)	C2B—C1B	1.44 (2)
C6A—H6A	0.9300	C2B—H2B	0.9300
C8B—C7B	1.291 (6)	C3B—C4B	1.36 (3)
C8B—C9	1.452 (5)	C3B—H3B	0.9300
C8B—H8B	0.9300	C5B—C6B	1.27 (3)
C9—O1	1.211 (3)	C5B—C4B	1.37 (3)
C9—O1^{i}	1.211 (3)	C5B—H5B	0.9300
C9—C8A	1.531 (6)	C1B—C6B	1.380 (9)
C9—C8A^{i}	1.531 (6)	C6B—H6B	0.9300
C1A—C7A	1.413 (11)	O1—O1^{i}	0.588 (10)
C5A—C4A—F1A	117.5 (19)	C2A—C3A—H3A	121.8
C5A—C4A—C3A	124 (2)	C8A—C7A—C1A	129.7 (6)
F1A—C4A—C3A	118 (2)	C8A—C7A—H7A	115.1

C4A—C5A—C6A	116.4 (18)	C1A—C7A—H7A	115.1
C4A—C5A—H5A	121.8	C8B—C7B—C1B	124.6 (6)
C6A—C5A—H5A	121.8	C8B—C7B—H7B	117.7
C1A—C2A—C3A	123.7 (17)	C1B—C7B—H7B	117.7
C1A—C2A—H2A	118.1	C7A—C8A—C9	119.8 (5)
C3A—C2A—H2A	118.1	C7A—C8A—H8A	120.1
C1A—C6A—C5A	119.6 (15)	C9—C8A—H8A	120.1
C1A—C6A—H6A	120.2	C3B—C2B—C1B	120.6 (18)
C5A—C6A—H6A	120.2	C3B—C2B—H2B	119.7
C7B—C8B—C9	127.4 (6)	C1B—C2B—H2B	119.7
C7B—C8B—H8B	116.3	C2B—C3B—C4B	119 (2)
C9—C8B—H8B	116.3	C2B—C3B—H3B	120.3
O1—C9—O1^{i}	28.1 (5)	C4B—C3B—H3B	120.3
O1—C9—C8B	93.5 (3)	C6B—C5B—C4B	120.9 (17)
O1^{i}—C9—C8B	121.6 (3)	C6B—C5B—H5B	119.6
O1—C9—C8B^{i}	121.6 (3)	C4B—C5B—H5B	119.6
O1^{i}—C9—C8B^{i}	93.5 (3)	C6B—C1B—C2B	116.4 (12)
O1—C9—C8A	120.8 (3)	C6B—C1B—C7B	119.2 (8)
O1^{i}—C9—C8A	148.4 (3)	C2B—C1B—C7B	124.0 (11)
O1—C9—C8A^{i}	148.4 (3)	C5B—C6B—C1B	121.6 (17)
O1^{i}—C9—C8A^{i}	120.8 (3)	C5B—C6B—H6B	119.2
C8A—C9—C8A^{i}	90.6 (4)	C1B—C6B—H6B	119.2
C2A—C1A—C7A	121.3 (12)	C3B—C4B—F1B	121.9 (18)
C2A—C1A—C6A	119.3 (13)	C3B—C4B—C5B	120.4 (18)
C7A—C1A—C6A	119.3 (10)	F1B—C4B—C5B	117.6 (19)
C4A—C3A—C2A	116.3 (19)	O1^{i}—O1—C9	76.0 (2)
C4A—C3A—H3A	121.8		

F1A—C4A—C5A—C6A	180.0 (12)	O1^{i}—C9—C8A—C7A	20.9 (13)
C3A—C4A—C5A—C6A	4 (3)	C8A^{i}—C9—C8A—C7A	−163.9 (4)
C4A—C5A—C6A—C1A	−2 (2)	C1B—C2B—C3B—C4B	−7 (3)
C7B—C8B—C9—O1	−169.9 (7)	C3B—C2B—C1B—C6B	7 (2)
C7B—C8B—C9—O1^{i}	−168.5 (8)	C3B—C2B—C1B—C7B	179.7 (13)
C7B—C8B—C9—C8B^{i}	10.8 (3)	C8B—C7B—C1B—C6B	−162.7 (7)
C3A—C2A—C1A—C7A	175.8 (13)	C8B—C7B—C1B—C2B	24.7 (13)
C3A—C2A—C1A—C6A	−6 (2)	C4B—C5B—C6B—C1B	6 (2)
C5A—C6A—C1A—C2A	3.8 (18)	C2B—C1B—C6B—C5B	−6.2 (18)
C5A—C6A—C1A—C7A	−178.3 (10)	C7B—C1B—C6B—C5B	−179.4 (11)
C5A—C4A—C3A—C2A	−6 (3)	C2B—C3B—C4B—F1B	−176.3 (16)
F1A—C4A—C3A—C2A	177.9 (13)	C2B—C3B—C4B—C5B	7 (3)
C1A—C2A—C3A—C4A	7 (3)	C6B—C5B—C4B—C3B	−6 (3)
C2A—C1A—C7A—C8A	−165.4 (11)	C6B—C5B—C4B—F1B	176.9 (14)
C6A—C1A—C7A—C8A	16.8 (10)	C8B—C9—O1—O1^{i}	178 (3)
C9—C8B—C7B—C1B	177.1 (4)	C8B^{i}—C9—O1—O1^{i}	−3 (3)
C1A—C7A—C8A—C9	−179.6 (5)	C8A—C9—O1—O1^{i}	171 (2)
O1—C9—C8A—C7A	13.2 (8)	C8A^{i}—C9—O1—O1^{i}	−14 (4)

Symmetry code: (i) −*x*+1, *y*, −*z*+1/2.

Hydrogen-bond geometry (Å, º)

D—H···*A*	*D*—H	H···*A*	*D*···*A*	*D*—H···*A*
C3*A*—H3*A*···F1*A*^{ii}	0.93	2.59	3.437 (17)	151
C3*A*—H3*A*···F1*B*^{ii}	0.93	2.66	3.477 (17)	146
C3*B*—H3*B*···F1*A*^{ii}	0.93	2.82	3.563 (19)	138
C3*B*—H3*B*···F1*B*^{ii}	0.93	2.71	3.519 (19)	146
C7*B*—H7*B*···O1^{iii}	0.93	2.84	3.745 (6)	163
C7*B*—H7*B*···O1^{iv}	0.93	2.59	3.448 (4)	154

Symmetry codes: (ii) −*x*+3/2, *y*+1/2, −*z*+1/2; (iii) −*x*+1, *y*−1, −*z*+1/2; (iv) *x*, *y*−1, *z*.